

**Metallic states induced by quantum lattice fluctuations**

Norikazu Tomita

*Department of Physics, Yamagata University, 1-4-12 Kojirakawa, Yamagata 990-8560, Japan*

Akira Takahashi

*Graduate School of Engineering, Nagoya Institute of Technology, Gokiso-Cho, Showa-ku, Nagoya 466-8555, Japan*

(Received 6 September 2018; revised manuscript received 10 December 2018; published 16 January 2019)

We developed a tractable many-body theory in which quantum lattice fluctuations beyond the adiabatic approximation, as well as electronic fluctuations, can be described. A many-body wave function is constructed by the superposition of direct products of Slater determinants for the electrons and the coherent states of phonons. The method was applied to a one-dimensional electron system with Su-Schrieffer-Heeger electron-phonon coupling. We show that, in the heavily doped regime, the quantum lattice fluctuations due to the collective motion of charged solitons cause a power-law singularity in the wave-number dependence of the electron density  $n_k$  at the Fermi wave number  $k = k_F$ . This indicates that a metallic state is induced by heavy doping, and it is a Tomonaga-Luttinger liquid. The current results can solve a long-standing problem for the electronic state of heavily doped polyacetylene, the coexistence of Pauli paramagnetism along with a strong infrared-active light absorption.

DOI: [10.1103/PhysRevB.99.035203](https://doi.org/10.1103/PhysRevB.99.035203)**I. INTRODUCTION**

Conducting polymers have a long history of significant contributions to technology. Nevertheless, the mechanism of their conductivity is still not well understood. Let us take trans-polyacetylene as an example. This material has a one-dimensional dimerized lattice at half filling due to  $2k_F$  nesting, which is called a Peierls instability. As a result, the band is doubly folded, and a Peierls gap opens at the Fermi wave number  $k_F$ . Thus, pristine polyacetylene is a semiconductor, but its conductivity dramatically increases with doping [1]. One of the most mysterious features of polyacetylene is that it does not show Pauli susceptibility in the lightly doped regime, at which point its conductivity almost reaches the level of a metal. A dimerized lattice has doubly degenerate alternating phases, such as (short bond)-(long bond)-(short bond)... or (long bond)-(short bond)-(long bond)... Therefore, there exist topological defects, called solitons, that convert alternating phases into each other. Interestingly, a charged soliton has a net charge of  $e$  but no spin, while a neutral soliton has no charge but  $\frac{1}{2}$  spin [2]. In other words, spin-charge separation is realized in these solitons on a one-dimensional lattice. In addition to this lack of Pauli susceptibility, infrared (IR) absorption experiments [3] show that the carriers are charged solitons in the lightly doped regime. On the other hand, polyacetylene shows Pauli susceptibility in the heavily doped regime [4], which strongly suggests that it acts as a normal metal. In fact, variational Monte Carlo (VMC) simulation [5] and density-matrix renormalization-group (DMRG) [6] calculations have suggested that the lattice dimerization vanishes in the heavily doped regime mainly due to electron correlation effects, and the system becomes a simple metal. However, optical experiments show that polyacetylene still has a strong IR component, whose intensity is proportional to the doping

ratio [7]. This result indicates that charged solitons survive heavy doping. As mentioned above, a soliton is a topological defect that changes the phase of lattice dimerization. Therefore, the persistence of solitons means that lattice dimerization is maintained in the heavily doped regime, which contradicts the above-mentioned theoretical predictions. Thus, the lattice structure and mechanism of conductivity in polyacetylene have been open questions for a long time. Similarly, in other conducting polymers, it is unclear how they become metallic by doping [8,9].

One of the most difficult aspects in describing conducting polymers is the strong electron-phonon coupling. In fact, their lattice structures easily change by doping. To date, such lattice structures have been described adiabatically by the Hellmann-Feynman theorem. Usually, this adiabatic treatment is relatively accurate, because the energy scale of phonons is smaller than that of electrons. However, in conducting polymers, lattice solitons (or polarons) form a band inside the gap between the valence and conduction bands. As a result, the gap between the valence (or conduction) and soliton (or polaron) bands becomes very small especially in the heavily doped regime. In light of this situation, it is better to treat the lattice quantum mechanically and go beyond the adiabatic approximation, because the lattice can fluctuate significantly in real materials. One of the authors (A.T.) suggested that a quantum-mechanical treatment of the lattice would be important for understanding the metallic nature of polyacetylene using quantum Monte Carlo (QMC) simulations [10]. In that research, however, the nonadiabatic effects of the lattice were only partially included, and the QMC calculations could not give clear results on the metallic state or quantum lattice fluctuations. Recently, we developed a tractable many-body theory which describes quantum lattice fluctuations beyond the adiabatic approximation [11]. The lattice is treated

quantum mechanically using a coherent-state representation, and nonadiabatic effects are included using the superposition of different coherent states. This is an extension of the resonating Hartree-Fock (Res-HF) approximation. In previous Res-HF wave functions, the electron correlation effects were described by the superposition of nonorthogonal Slater determinants [12]. We could visualize the quantum electronic fluctuations by analyzing the Slater determinants. On the other hand, in the present Res-HF theory, we can directly see quantum lattice fluctuations, as well as quantum electronic fluctuations, by analyzing the coherent states and Slater determinants.

In the present paper, we try to clarify the lattice and electronic structure of polyacetylene. In particular, the goal is to understand the doping dependence of the carriers and the lattice structures in the framework of quantum mechanics, beyond the adiabatic approximation. Through such doping dependence, we can reasonably understand the IR and Pauli paramagnetic susceptibility experiments. We calculate the wave-number dependence of the electron density  $n_k$ , to find if the carriers have a Tomonaga-Luttinger liquid (TLL) contribution or not. In a TLL (a Fermi liquid),  $n_k$  has a power-law singularity (a jump) at the Fermi wave number  $k_F$  [13], while  $n_k$  has neither a power-law singularity nor a jump at  $k_F$  in an insulator. We will show that  $n_k$  changes gradually around  $k_F$  in the lightly doped regime, which indicates that the carriers are not simple holes (or electrons). In fact, from the structures of the Slater determinants and coherent states, we will see that the carriers are charged lattice solitons, which is consistent with previous work [3]. On the other hand,  $n_k$  shows an abrupt change with a singularity at  $k_F$  in the heavily doped regime, which indicates that the heavily doped state is a TLL. The critical exponent for  $n_k$  in the vicinity of  $k = k_F$ , characteristic of a TLL, is roughly estimated to be 0.23 at 16% hole doping. We should note that a TLL in one dimension can produce the Pauli susceptibility seen in Fermi liquids in higher dimensions [13]. Furthermore, from the structures of the Slater determinants and coherent states, we can see directly that charged solitons survive heavy doping. Therefore, the strong IR components can be explained by charged solitons, even in the heavily doped regime. We propose that the quantum lattice fluctuations beyond the adiabatic approximation close the gap between the valence (or conduction) and soliton bands, and as a result, the system has a TLL contribution even with charged lattice solitons. These results can explain the Pauli paramagnetic susceptibility and IR experiments consistently.

The present paper is organized as follows. The theoretical framework is introduced in Sec. II. The results and discussion are given in Sec. III. Finally, we give a brief summary in Sec. IV.

## II. METHODS AND MODEL

In this research, the lattice is treated quantum mechanically using a coherent-state representation, which is given by

$$|\phi\rangle = e^{-|z|^2/2} e^{z \cdot \mathbf{b}^\dagger} |0\rangle, \quad (1)$$

where  $|0\rangle$  is vacuum of phonons.  $\mathbf{z} = \{z_k\}$  is a probability amplitude for the corresponding phonon mode represented by  $\mathbf{b}^\dagger = \{b_k^\dagger\}$ , where  $-\pi \leq k < \pi$ . These phonon modes constitute the basis set to describe the lattice quantum mechanically.

In the following one-dimensional system, we set the uniform equidistant lattice as the corresponding crystal structure. Then, displacements from the corresponding structure and momentum of  $n$ th site can be described using the second quantization form:

$$q_n = \sum_k \sqrt{\frac{\hbar}{2MN\omega(k)}} (b_k + b_{-k}^\dagger) e^{ikn}, \quad (2)$$

$$p_n = i \sum_k \sqrt{\frac{M\hbar\omega(k)}{2N}} (b_k^\dagger - b_{-k}) e^{-ikn}, \quad (3)$$

where  $\omega(k) = 2(K/M)^{1/2} |\sin k/2|$ . The lattice points can deviate from their equidistant positions, but they never leave the solid, which leads to

$$\langle \phi | p_n | \phi \rangle = i \sum_k \sqrt{\frac{M\hbar\omega(k)}{2N}} (z_k^* - z_{-k}) e^{-ikn} = 0. \quad (4)$$

Here, we use the fact that the coherent state is an eigenstate of the annihilation operator, such that

$$b_k |\phi\rangle = b_k e^{-|z|^2/2} e^{z \cdot \mathbf{b}^\dagger} |0\rangle = z_k |\phi\rangle. \quad (5)$$

From Eq. (4), we obtain

$$z_k^* = z_{-k}. \quad (6)$$

Then, the lattice displacement is given by

$$\begin{aligned} \langle \phi | q_n | \phi \rangle &= \sum_k \sqrt{\frac{\hbar}{2MN\omega(k)}} (z_k + z_{-k}^*) e^{ikn} \\ &= \sum_k \sqrt{\frac{2\hbar}{MN\omega(k)}} z_k e^{ikn}. \end{aligned} \quad (7)$$

Thus, probability amplitude  $\{z_k\}$  is directly related to the lattice displacement  $\{q_n\}$ .

Now, we show how to apply this coherent-state representation. In the following, we employ the extended Hubbard model with Su-Schrieffer-Heeger (SSH) electron-phonon coupling [2], in which the Hamiltonian is given by

$$\begin{aligned} H &= H_{SSH} + H_{ph} + H_{e-e} \\ &= - \sum_{i,\sigma}^N (t - \alpha X_i) (c_{i+1,\sigma}^\dagger c_{i,\sigma} + c_{i,\sigma}^\dagger c_{i+1,\sigma}) \\ &\quad + \sum_i^N \left[ \frac{1}{2M} p_i^2 + \frac{K}{2} X_i^2 \right] \\ &\quad + U \sum_i^N n_{i,\uparrow} n_{i,\downarrow} + V \sum_i^N n_{i+1} n_i, \end{aligned} \quad (8)$$

$$X_i = q_{i+1} - q_i, \quad (9)$$

where  $c_{i,\sigma}^\dagger (c_{i,\sigma})$  represents a creation (annihilation) operator for an electron with spin  $\sigma$  at the  $i$ th site, while  $n_{i,\sigma} = c_{i,\sigma}^\dagger c_{i,\sigma}$  and  $n_i = n_{i,\uparrow} + n_{i,\downarrow}$ . Here, we impose a periodic boundary condition. This periodic ring has  $D_N$  symmetry, where  $N$  represents the system size. The parameters  $t$ ,  $U$ , and  $V$  denote the hopping integral for the nearest-neighbor

sites of the uniform equidistant lattice, the on-site, and the nearest-neighbor Coulomb interactions, respectively.  $\alpha$  and  $K$  represent the electron-lattice interaction parameter and spring constant, respectively, while  $M$  is the mass of a lattice point. This model is often used to investigate trans-polyacetylene, in which the lattice points are carbon atoms. When an atom moves from its equidistant position, its bonds with neighboring atoms lengthen or shorten, and the electron hopping integrals of the bonds change. This bond-length dependence of the electron hopping integral is included up to the first order in the deviation  $X_i$ . These  $\{q_i\}$  and  $\{p_i\}$  are treated quantum mechanically, as shown in Eqs. (2) and (3).

For the electron-phonon coupled system, the wave function is constructed using the superposition of direct products of Slater determinants for electrons and the coherent states of phonons. In the present Res-HF method, we approximate this using the superposition of a finite number ( $N_S$ ) of direct products of the following form:

$$|\Psi\rangle = \sum_P \sum_{f=1}^{N_S} C_f \hat{P} |\psi_f\rangle |\phi_f\rangle = \sum_P \sum_{f=1}^{N_S} C_f \hat{P} |\psi_f \phi_f\rangle, \quad (10)$$

where  $|\psi_f\rangle$ 's represent the Slater determinants for electrons while  $|\phi_f\rangle$ 's denote the coherent states of phonons.  $C_f$ 's are the superposition coefficients. In the Res-HF method, we employ the unrestricted Hartree-Fock (UHF) symmetry-broken Slater determinants and coherent states. Each Slater determinant (and coherent state) is nonorthogonal to the others. The large quantum fluctuations are effectively described by using such nonorthogonal Slater determinants (and coherent states). Because the true many-body wave function should possess the original symmetry of the system represented by  $D_N$ , we carry out symmetry projections, schematically represented by  $\hat{P}$  in Eq. (10). When we apply the spatial symmetry projections, the electronic states and the lattice are simultaneously translated and rotated. In the case of  $N_S = 1$ , it becomes the Hartree-Fock (HF) approximation, especially if we do not adopt the symmetry projections  $\hat{P}$ . On the other hand, in the case of  $N_S \geq 2$ , different electron-phonon coupled states are superposed, and the wave function can describe the quantum interference or quantum fluctuations. We should note that all of the Slater determinants and coherent states have their own independent orbitals and probability amplitudes, respectively. Therefore, nonadiabatic effects are naturally included in the Res-HF wave function. We optimize the orbitals for all the Slater determinants and the probability amplitudes in all the coherent states, as well as the superposition coefficients [11].

The expectation value of the energy is given by

$$E = \sum_{f,g} C_f C_g \langle \phi_f, \psi_f | H | \psi_g, \phi_g \rangle, \quad (11)$$

where we omit the symmetry projection operator for simplicity. This expectation value is divided into three terms:

$$\begin{aligned} \langle H_{SSH} \rangle_{fg} &= -t \langle \phi_f | \phi_g \rangle \sum_{i,\sigma} \langle \psi_f | h_{i,\sigma} | \psi_g \rangle \\ &+ \alpha \sum_{i,\sigma} \langle \phi_f | X_i | \phi_g \rangle \langle \psi_f | h_{i,\sigma} | \psi_g \rangle, \quad (12) \end{aligned}$$

$$\langle H_{ph} \rangle_{fg} = \langle \phi_f, \psi_f | \psi_g, \phi_g \rangle \sum_k \hbar \omega_k z_{f,k}^* z_{g,k}, \quad (13)$$

$$\langle H_{e-e} \rangle_{fg} = \langle \phi_f | \phi_g \rangle \sum_i \langle \psi_f | U n_{i,\uparrow} n_{i,\downarrow} + V n_i n_{i+1} | \psi_g \rangle, \quad (14)$$

where  $h_{i,\sigma} = c_{i+1,\sigma}^\dagger c_{i,\sigma} + (\text{H.c.})$ . For practical calculations of the coherent states, we can use the relations

$$\langle \phi_f | \phi_g \rangle = e^{-\sum_k |z_{f,k} - z_{g,k}|^2 / 2}, \quad (15)$$

$$\begin{aligned} \langle \phi_f | q_n | \phi_g \rangle &= \sum_k \sqrt{\frac{\hbar}{2MN\omega(k)}} \langle \phi_f | (b_k + b_{-k}^\dagger) | \phi_g \rangle e^{ikn} \\ &= \sum_k \sqrt{\frac{\hbar}{2MN\omega(k)}} (z_{g,k} + z_{f,-k}^*) \langle \phi_f | \phi_g \rangle e^{ikn} \\ &= \sum_k \sqrt{\frac{\hbar}{2MN\omega(k)}} (z_{g,k} + z_{f,k}) \langle \phi_f | \phi_g \rangle e^{ikn} \\ &= \frac{\langle \phi_f | \phi_g \rangle}{2} [\langle \phi_f | q_n | \phi_f \rangle + \langle \phi_g | q_n | \phi_g \rangle], \quad (16) \end{aligned}$$

where we use Eqs. (2), (5), (6), and (7) to derive Eq. (16). Then, we obtain

$$\langle \phi_f | X_i | \phi_g \rangle = \frac{\langle \phi_f | \phi_g \rangle}{2} [\langle \phi_f | X_i | \phi_f \rangle + \langle \phi_g | X_i | \phi_g \rangle]. \quad (17)$$

Details of the optimization procedures can be found in previous work [11], where we clarified the quantum fluctuations in the charge density wave (CDW) ground state. One of the most important points is that the Slater determinants are optimized for the collective potential energy landscape created by all the coherent states, not individually. Thus, the present formalism naturally goes beyond the adiabatic approximation.

In previous papers, we demonstrated that the Res-HF method can well describe the electron correlation effects for the one- and two-dimensional Hubbard models without the electron-phonon coupling [14,15]. On the other hand, in the present system, many-body effects due to the electron-phonon coupling are also important. There are pioneering works which treat SSH electron-phonon coupling quantum mechanically using the DMRG [16] and QMC [17,18] methods. To check the accuracy of the present Res-HF method, we compare the ground-state energies at half filling. The ground-state energy using the DMRG method depends on the number of oscillator levels per site, and it changes from  $-58.440$  (single phonon per site) to  $-60.221$  (seven phonons per site) at half filling with  $N = 40$ ,  $\omega = t$ ,  $U = 4V = 2.5t$ , and  $g = \sqrt{\alpha^2/Kt} = 0.1$  [16]. On the other hand, the Res-HF energy for the ground state with  $N_S = 5$  generating Slater determinants and coherent states is  $-60.148$ . Thus, the Res-HF approximation gives 98% of the correlation energy (difference in energy from the HF ground state) calculated by DMRG, and we can safely say that the Res-HF method is a very good approximation to describe correlated systems with the electron-phonon coupling. Furthermore, for  $N_S \geq 3$ ,  $n_k$  very weakly depends on  $N_S$  as shown later, and this convergence behavior shows that the present Res-HF method with  $N_S = 5$  is reliable to calculate  $n_k$ .

### III. RESULTS AND DISCUSSION

Before showing our results, we define several physical quantities, through which we are able to analyze the lattice and electronic structure, including

$$\begin{aligned}
 Q_f(l) &= \langle \psi_f, \phi_f | q_l | \psi_f, \phi_f \rangle, \\
 CD_f(l) &= \langle \psi_f, \phi_f | \sum_{\sigma} (c_{l\sigma}^{\dagger} c_{l\sigma} - 1) | \psi_f, \phi_f \rangle, \\
 SD_f(l) &= \langle \psi_f, \phi_f | \sum_{\sigma} \sigma c_{l\sigma}^{\dagger} c_{l\sigma} | \psi_f, \phi_f \rangle.
 \end{aligned}$$

$Q_f(l)$  represents the lattice displacement from the corresponding equidistant position for the  $f$ th configuration, while  $CD_f(l)$  and  $SD_f(l)$  denote the charge and spin density, respectively. To see the lattice and electronic structure clearly, physical quantities, represented by  $O_f(l)$ , can be decomposed into their net (NO) and alternating (AO) components, as in

$$O_f(l) = NO_f(l) + (-1)^l AO_f(l). \quad (18)$$

In the following calculations, the energy is scaled by  $t$ .  $\alpha$  and  $K$  are set at 0.29 and 0.23, respectively, while  $\omega = 2(K/M)^{1/2}$  is set at 0.066. These values are reasonable for polyacetylene [2,19]. First, we show the structure of the wave function for  $U = V = 0$ . If we treat the lattice classically and determine the lattice displacements  $q_i$  adiabatically, we can easily diagonalize the Hamiltonian for  $U = V = 0$ . However, it gives the approximate classical adiabatic solution. This Hamiltonian cannot be exactly solved even for  $U = V = 0$ , if we treat the lattice quantum mechanically and go beyond the adiabatic approximation. We should note that this comes at the cost of a substantial increase in complexity. The model intrinsically includes a many-body problem because of the electron-

phonon coupling. In fact, we have shown in a previous paper that a quantum nonadiabatic treatment for the lattice yields a significantly lower ground-state energy, compared with a classical adiabatic treatment [11]. In the current calculations, we superpose five configurations ( $N_S = 5$ ), each of which is composed of direct product of a Slater determinant and the coherent state, to construct the many-body wave function. In Fig. 1, we show the lattice structure of the wave function at half filling ( $N = N_e = 198$ ). Here,  $N$  represents the system size, and  $N_e$  is the number of electrons. For the sake of brevity, the lattice structures of three typical configurations are shown. As mentioned above, the  $Q_f(l)$  values for the lattice structure are obtained from the optimized  $f$ th coherent state using Eq. (7). In this figure, a positive (negative)  $Q$  value denotes that the lattice point moves right (left). We can see that all of the optimized coherent states have dimerized lattices. Therefore, the ground state can be regarded as a bond order wave (BOW) state. However, from  $AQ$  values representing the amplitudes of the dimerization, it is clear that these lattices have some modulation compared with a uniform dimerization. Translation and inversion of each configuration along with superpositions of these configurations form the many-body wave function. There are no significant spin or charge components, though they are omitted from Fig. 1. Thus, the quantum fluctuations can be primarily described by the translational motion of these modulations from the uniform lattice in the case of half filling. Much larger defects, such as lattice solitons, do not play an important role in this case.

Next, we show in Fig. 2 the lattice and electronic structure for the wave function with  $N = 198$  and  $N_e = 194$ , which corresponds to approximately 2% hole doping. The wave function is also composed of five configurations, and

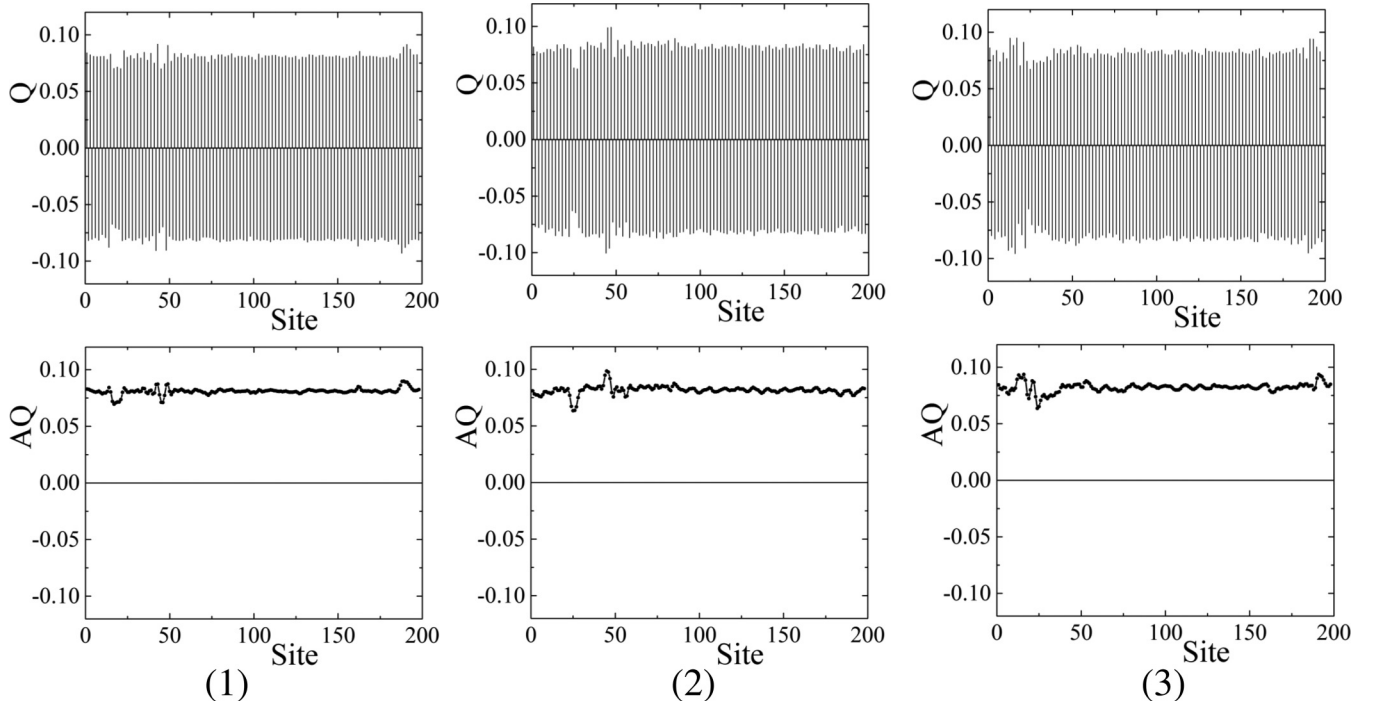


FIG. 1. Lattice structures for three of the five coherent states superposed to generate the wave function at half filling.

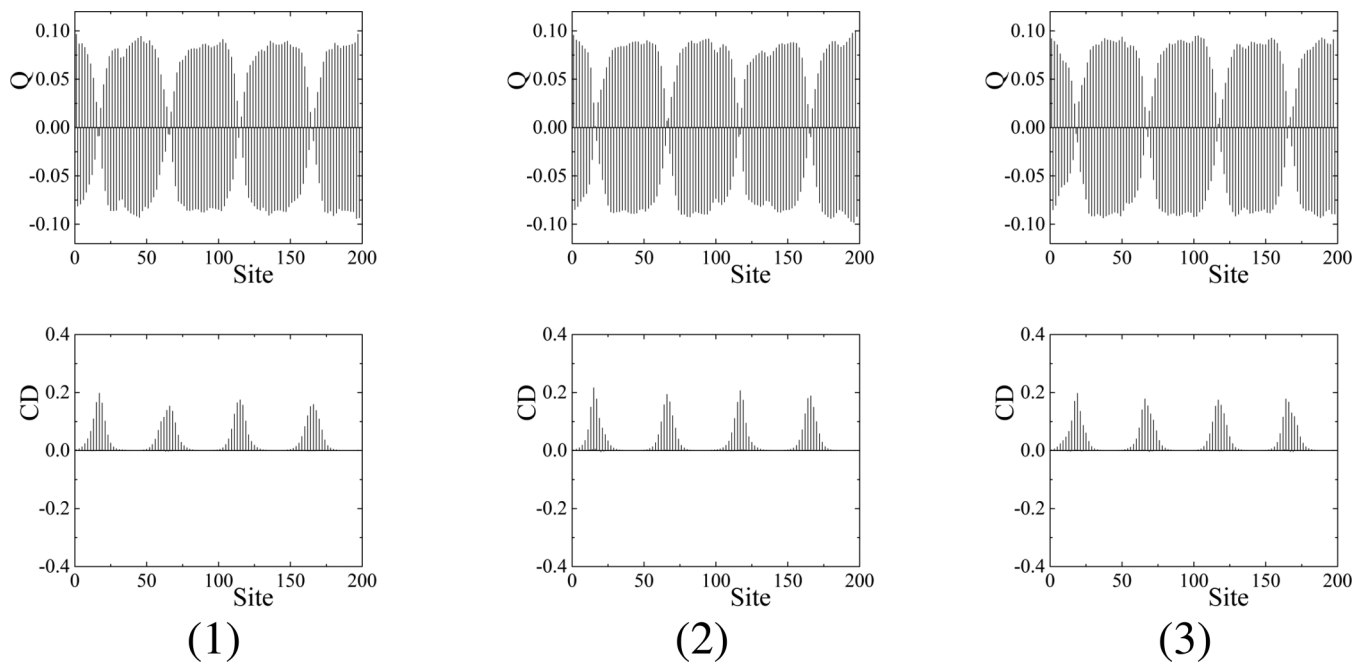


FIG. 2. Lattice and electronic structures for three of the five coherent states superposed to generate the wave function at  $N = 198$  and  $N_e = 194$ .

we show the structures of three typical examples. All of the lattices deviate largely from uniform dimerization, and significant charge components appear. To investigate these structures more closely, the alternating components of the lattice displacements ( $AQ$ ) and charge densities (ACD), as well as the net components of the charge densities (NCD), are shown in Fig. 3. The configurations are the same as in Fig. 2. All of the  $AQ$  values change their signs four times, which corresponds to the number of holes. The ACD and NCD components arise where the  $AQ$  values change signs. We can consider the lattice and electronic structures shown in Figs. 2 and 3 as charged lattice solitons, since they convert the phase of the dimerization, and have net charge but no spin. It should be noted that the present calculation is not a simple HF approximation, but a nonorthogonal multiconfiguration approach. As a result, the character of the charged soliton from the HF approximation appears to be slightly modified. Nevertheless, we can safely conclude that doped holes become charged lattice solitons. To observe the essential quantum fluctuations, we show the  $AQ$  components of all five configurations in Fig. 4. In this figure, the lattice points are shifted so that the first soliton occurs at the 17th site. We can see that the distances between solitons are different in different configurations. These differences lead to the quantum vibrational (breathing) motion of solitons. Thus, quantum fluctuations in the present lightly doped system can be primarily described by the translational and vibrational motions of the charged lattice solitons.

Here, we briefly mention the difference between the present results and previous ones in Ref. [11]. In the previous paper, we investigated the quantum fluctuations in the CDW ground state. When we dope the CDW state, charged CDW solitons are formed. These charged CDW solitons induce the BOW-like structure around the soliton centers. On the other hand, in the present studies, the BOW state is the ground

state, and charged lattice solitons are created by doping. These charged lattice solitons induce the CDW-like structure around the soliton centers. As a result, in both cases, the BOW and CDW structures are coexisting. They look quite similar but we should note that they are physically different. In the present paper, we are investigating quantum fluctuations in the BOW state by changing the doping ratio.

Moving to a heavily doped system, Fig. 5 shows the lattice and electronic structures for  $N = 198$  and  $N_e = 166$ , which corresponds to approximately 16% hole doping. The wave function is constructed using five configurations, and we show the lattice and electronic structures of four typical configurations. First, from  $AQ$  and ACD values in Fig. 5(1), we can see that 32 lattice solitons occur in this configuration. The structures of the NCD are rescaled in the second panel of the right column, and it can be seen that the charge comes primarily from the lattice solitons. This configuration also contains extra structures between sites 196 and 5 (wrapped around due to the periodic boundary condition). The SD and NCD show that this defect has both spin and charge components. Although we did not find clear HF states corresponding to these structures, we can suggest that they would be an electronic polaron-antipolaron pair inside the charged lattice solitons. The charged lattice solitons induce a charge density wave (CDW) regime and a polaron-antipolaron pair appear in this CDW regime. In fact, the electronic polaron is known to induce spin density waves (SDWs) and bond order waves (BOWs) in the CDW regime [20]. If this induced BOW matches (or mismatches) the alternating phase of the lattice dimerization, the  $AQ$  is enhanced (or suppressed). We can see such an electronic polaron-antipolaron pair in Figs. 5(3) and 5(4). Polarons or bipolarons are often observed in nondegenerate systems, while the present model has degenerate alternating phases for the lattice dimerization. Therefore, finding quantum fluctuations due to polaron pairs

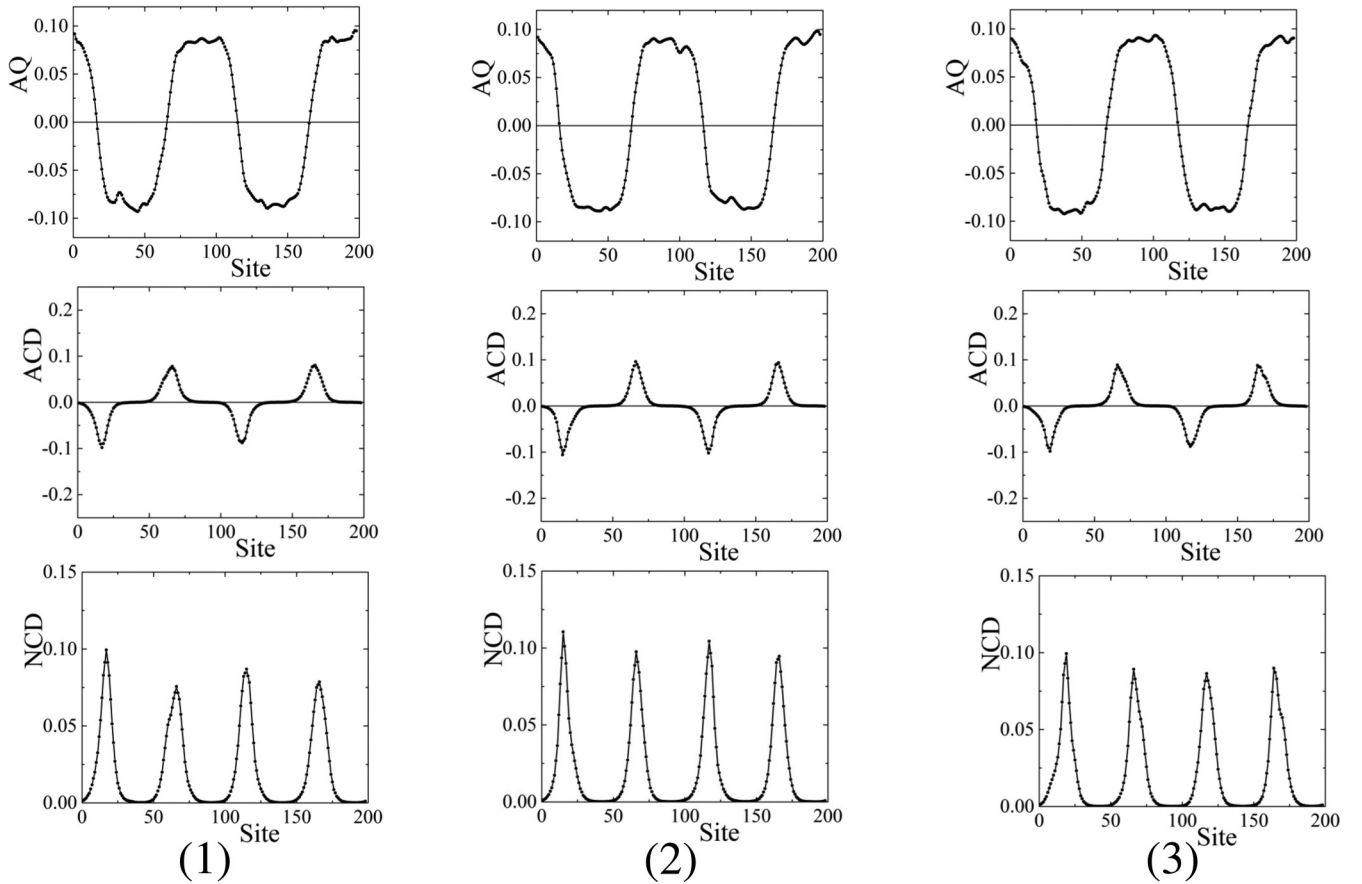


FIG. 3. Alternating components of the lattice structure (upper panel), and alternating and net components of the charge density (middle and lower panels, respectively) with  $N = 198$  and  $N_e = 194$ . The coherent states and Slater determinants in Fig. 2 are decomposed.

is interesting. However, the contributions of the polarons to the total charge are small, and such quantum fluctuations will play a minor role, compared with those of the charged solitons. In fact, Figs. 5(2)–5(4) show that lattice solitons are also formed in these configurations, and they dominate the total charge calculations. The distances between solitons are different in different configurations. Furthermore, the shapes of the solitons are also different. These differences, as well as the translation of solitons, cause the dominant quantum fluctuations in the system.

These solitons are very important when explaining the result of IR experiments. The IR intensity cannot be from a uniform charge distribution, as in a simple metal, but requires a spatially dense and sparse distribution of charge. As shown above, the charged solitons produce such a charge distribution. Therefore, the persistence of the charged solitons accords with the IR experiments. Furthermore, our results show that the number of solitons increases linearly with doping. In fact, the experimentally observed IR intensity also increases proportionally with the doping ratio [4]. Thus, the current

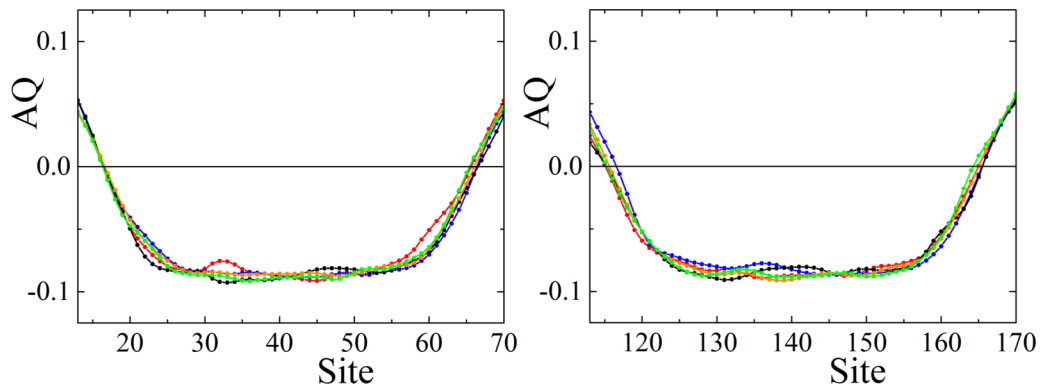


FIG. 4. Alternating components of the lattice structure for all five configurations. We focus on the lattice points where the AQ value changes sign.

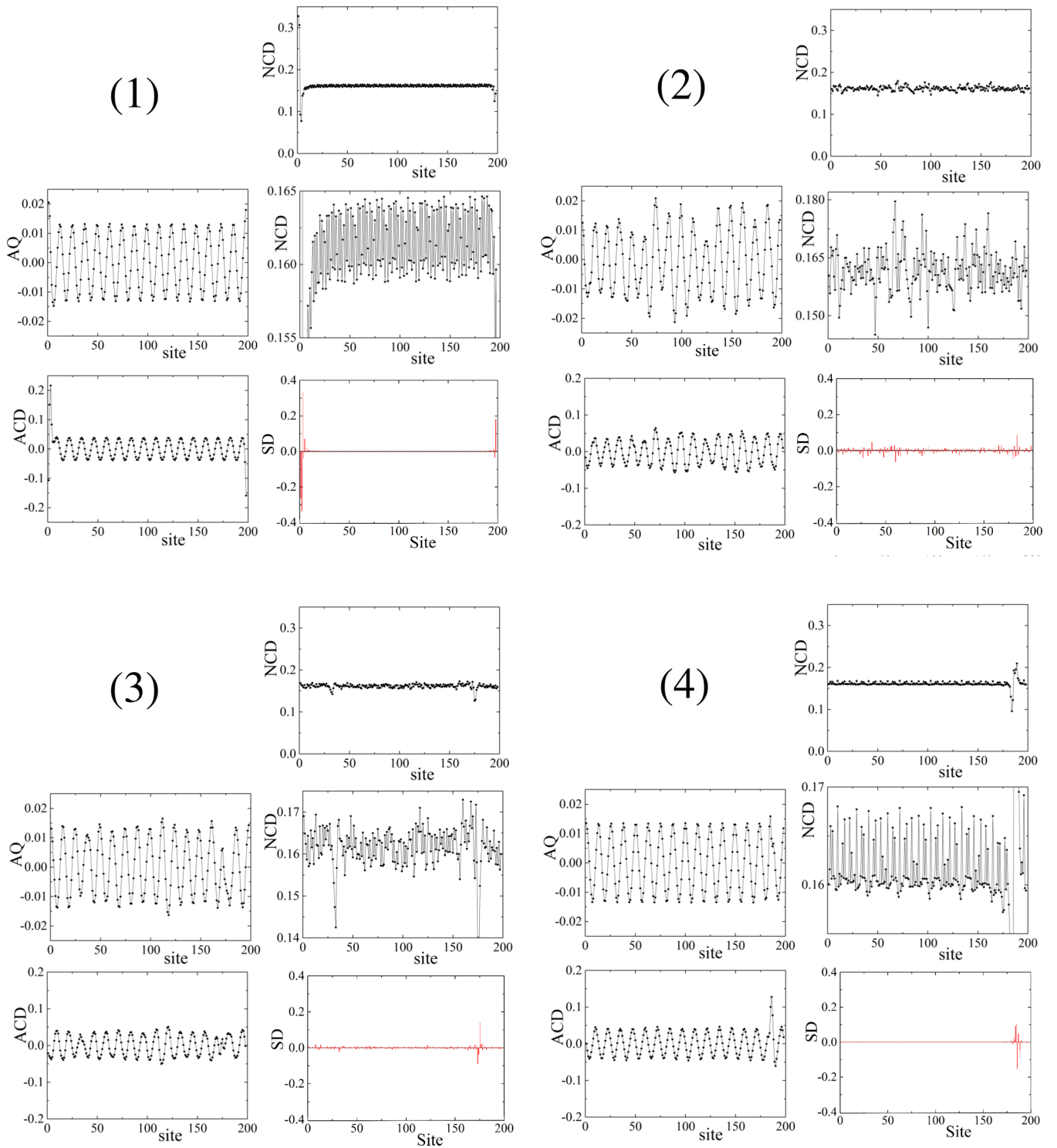


FIG. 5. Alternating components of the lattice structure and charge density (left panels), overall and rescaled net components of the charge density (upper and middle panels right, respectively), and the spin density (right bottom panel) at  $N = 198$ ,  $N_e = 166$ .

results are consistent with the IR experiments on doped polyacetylene.

One of the most serious inconsistencies with IR experiments is the measured Pauli susceptibility. In the heavily doped regime of polyacetylene, a finite Pauli susceptibility has been observed [4]. A TLL in one dimension can yield such a Pauli susceptibility, but charged solitons cannot. Recall that

charged solitons do not have a spin component. Therefore, the origin of the Pauli susceptibility has been debated for a long time. In this research, we show the possibility that the quantum fluctuations due to the charged lattice solitons create a significant TLL component in the doped system. Figure 6 shows the doping dependence of  $n_k$ . Here,  $n_k$  represents the momentum dependence of the electron density, which is

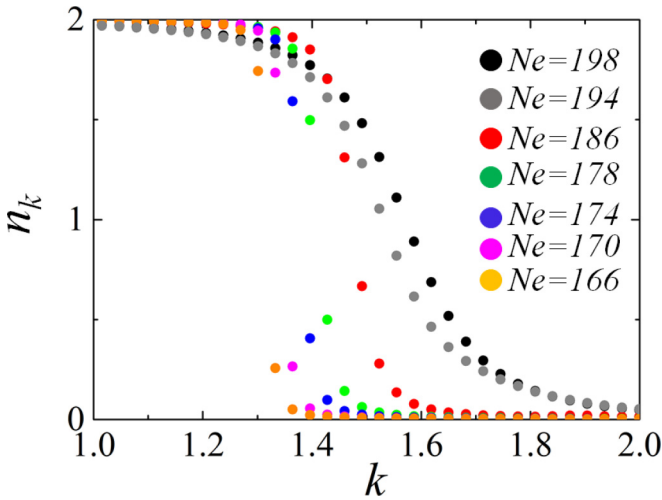


FIG. 6. Doping dependence of  $n_k$  for  $N = 198$ .  $k_F$  is given by  $\frac{N_e\pi}{2N}$ .

defined by

$$n_k = \frac{1}{N} \sum_{l,l',\sigma} \langle \Psi | c_{l,\sigma}^\dagger c_{l',\sigma} e^{-ik(l-l')} | \Psi \rangle. \quad (19)$$

When there are no interactions or lattice distortions, the system has a metallic band without ever exhibiting a gap. In such a case, the momentum is a good quantum number to determine the state of electrons, and the quasiparticles are just bare free electrons. At zero temperature, as is being considered here, the  $n_k$  values show a jump at the Fermi wave number. When the electron-electron or electron-phonon interactions are switched on in the system, the quasiparticle loses its free-electron component. As a result, the jump in  $n_k$  at the Fermi wave number decreases. If the system becomes an insulator,  $n_k$  is analytic even at  $k = k_F$  without a singularity. On the other hand, if the system is a metal,  $n_k$  values show a singularity at  $k = k_F$ . In the case of one-dimensional systems, such a metallic state is believed to be a TLL. Thus, instead of measuring the band gap itself, which is quite complicated to determine in the correlated systems, we focus on the doping

dependence of  $n_k$ , which gives important information on the electronic states of the system. If  $n_k$  shows an abrupt singular change and does not show a jump at the Fermi wave number, the electrons there must possess significant TLL components, and we can conclude that the system is metallic.

Now, we turn to Fig. 6. In the case of half filling (black circles),  $n_k$  changes very gradually at the Fermi wave number. In this case, as is well known, a Peierls gap opens at the Fermi wave number due to perfect nesting. This Peierls mechanism is essentially the same as with the usual band-gap formation due to the nesting of the reciprocal vectors. The original free-electron component is drastically reduced by the mixing of states connected by the  $2k_F$  reciprocal vectors. As a result,  $n_k$  does not possess a singular component at the Fermi wave number. Thus, the current situation with  $n_k$  that gradually changes at the Fermi wave number corresponds to a Peierls insulator at a half filled system. The change in  $n_k$  at the Fermi wave number is still gradual in the case of  $N_e = 194$ , which corresponds to approximately 2% doping. It starts to show an abrupt change at the Fermi wave number when  $N_e$  is less than 186. In the case of heavy doping, like  $N_e = 170$  and 166,  $n_k$  shows a very steep change at the Fermi wave number, which suggests that the carriers have large TLL contributions. Therefore, the present result suggests that the system becomes metallic in the heavily doped regime.

To see how critically  $n_k$  changes at  $k = k_F$ , we show the system size dependence of the first- and second-order derivatives of  $n_k$  at  $k = k_F$  in Figs. 7(a) and 7(b), respectively. In these figures,  $\rho$  represents  $N_e/N$ , and the hole-doping ratio corresponds to  $1 - \rho$ . For each  $\rho$ , we choose several sets of  $N$  and  $N_e$ , whose ratio  $N_e/N$  become  $\rho$  up to the second decimal place. In the half filled (black circles) and 2% doped (gray circles) cases, the first-order derivatives are saturated and the second-order derivatives go to zero as the system size increases. This indicates that  $n_k$  is a smooth function, and  $k = k_F$  is a normal inflection point in the half filled and lightly doped cases. On the other hand, the first-order derivatives keep increasing with increasing system size, for  $\rho \leq 0.94$ . Furthermore, the second-order derivatives also keep increasing in these cases. These results show that both the first- and second-order derivatives diverge at  $k = k_F$ , which indicates

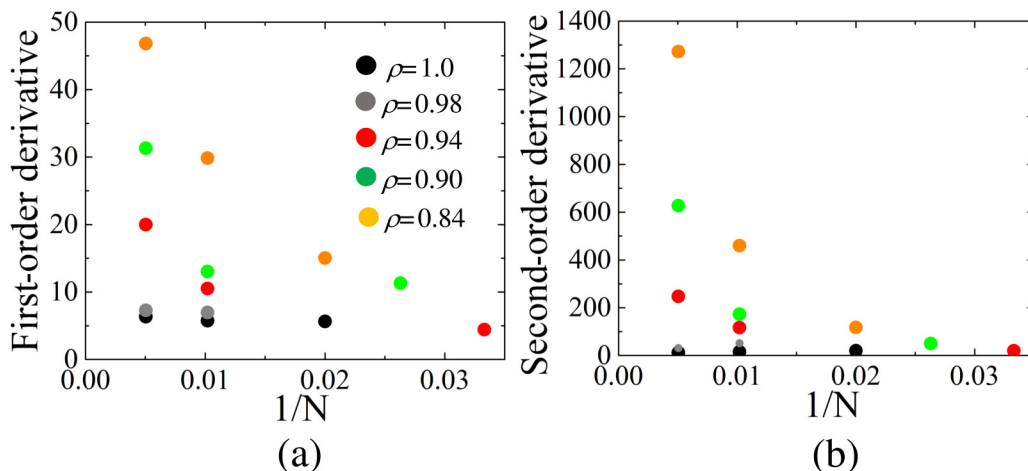


FIG. 7. Size dependence of the absolute values of the first-order (a) and second-order (b) derivatives of  $n_k$  at  $k = k_F$  for  $U = V = 0$ .

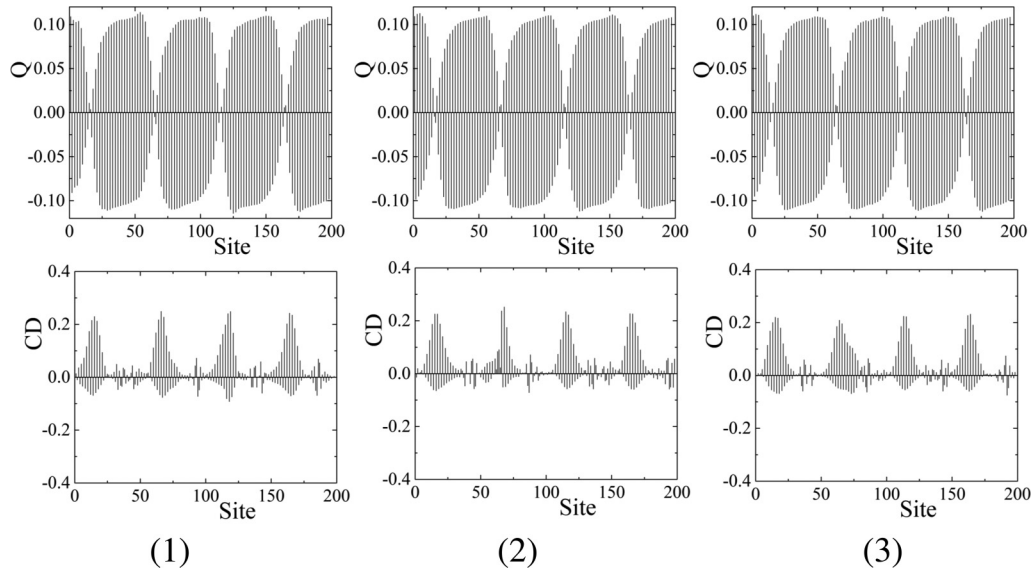


FIG. 8. Lattice and electronic structures of three of the five coherent states superposed to generate the wave function for  $(U, V) = (1.0, 0.5)$  at  $N = 198$  and  $N_e = 194$ .

that  $n_k$  has a singularity at  $k = k_F$  in the heavily doped regime. From the critical behavior in  $n_k$  at  $k = k_F$ , shown above, we can conclude that the system becomes a TLL or a Fermi liquid. However, the possibility of a Fermi liquid can be excluded as shown later. We should note that a TLL can contribute to the Pauli susceptibility [13]. The role of electron-correlation effects in polyacetylene has been a debating issue for a long time. In the present research, we demonstrated that the electron-phonon coupled system can be metallic in the heavily doped regime without electron-correlation effects. Our results for  $U = V = 0$ , shown above, indicated that the quantum lattice fluctuations due to the collective motion of the charged solitons lead to a metallic ground state, which gives rise to both the observed Pauli susceptibility and the IR response.

Next, we show results for  $U = 1.0, V = 0.5$ . First, we clarify the differences in the structures of solitons. In the case of  $U = V = 0$ , as shown in Fig. 2, CD does not have any negative components where solitons are created. These are called amplitude solitons. To compare the structures of the solitons, we show the lattice movements  $Q$  and CD for  $U = 1.0, V = 0.5$  with  $N_e = 194$  (the same number of electrons as in Fig. 2) in Fig. 8. We can see the negative components of CD where the solitons are created. These are called phase solitons. Sasai and Fukutome pointed out that only phase solitons can explain the results of x-ray photoelectron spectroscopy (XPS) and NMR experiments on polyacetylene [21,22]. Thus, the Coulomb interaction is important in polyacetylene. On the other hand, in our calculation, the lattice becomes equidistant, and the solitons disappear, when the Coulomb interactions are large ( $U \geq 1.5$ ), which is consistent with previous DMRG results [6]. The state with an equidistant lattice and no lattice solitons is a simple metal, which explains the measured Pauli susceptibility. However, the simple metal on an equidistant lattice cannot explain the IR experiments. Thus, the strong (or even intermediate) electron-correlation effects do not produce a reasonable ground state for polyacetylene. We suggest

that the Coulomb parameters for polyacetylene must lie in a very small range, with finite but small  $U$  and  $V$  values, which is consistent with previous work [23]. In the case of  $U = 1.0, V = 0.5$ , the doping dependence of the lattice and electronic structure is qualitatively the same as for  $U = V = 0$ , though the structures of the solitons are different. We show the size dependence of the first- and second-order derivatives of  $n_k$  for  $U = 1.0, V = 0.5$  in Fig. 9, which are also qualitatively the same as in Fig. 7. Thus, we can conclude that polyacetylene can be metallic with phase solitons.

Here, we discuss whether the metallic state of polyacetylene is really a TLL. In the case of a TLL,  $n_k$  has a singularity at  $k = k_F$  given by

$$\lim_{k \rightarrow k_F} |n_{k_F} - n_k| = C|k_F - k|^\alpha, \quad (20)$$

where the critical exponent  $\alpha (< 1)$  depends on the system and doping ratio for the one-dimensional Hubbard model. On the other hand, in the case of a Fermi liquid,  $n_k$  has a jump at  $k = k_F$  whose amplitude corresponds to the weight of the coherent component in the quasiparticle. Therefore,

$$\lim_{k \rightarrow k_F} |n_{k_F} - n_k| = \text{const.} \quad (21)$$

In the case of an insulator,  $n_k$  is differentiable at  $k = k_F$ , and therefore

$$\lim_{k \rightarrow k_F} |n_{k_F} - n_k| = \left. \frac{dn_k}{dk} \right|_{k=k_F} \times |k_F - k|. \quad (22)$$

Thus,  $n_k$  of a TLL, a Fermi liquid, and an insulator show different behaviors in the vicinity of  $k = k_F$ . Figure 10 shows the  $|k_F - k|$  dependence of  $|n_{k_F} - n_k|$  for  $N = 198, N_e = 166$ , and  $(U, V) = (1.0, 0.5)$  in log-log scale. By taking two points nearest to  $k_F$ , we obtain  $\alpha = 0.23$ . If the system is a Fermi liquid,  $\alpha$  should be 0, or  $\alpha$  should be 1 if the system is an insulator. The obtained value of  $\alpha = 0.23$  clearly shows that the system is a TLL. It is difficult to determine the critical exponent  $\alpha$  precisely. However, in the present calculations,

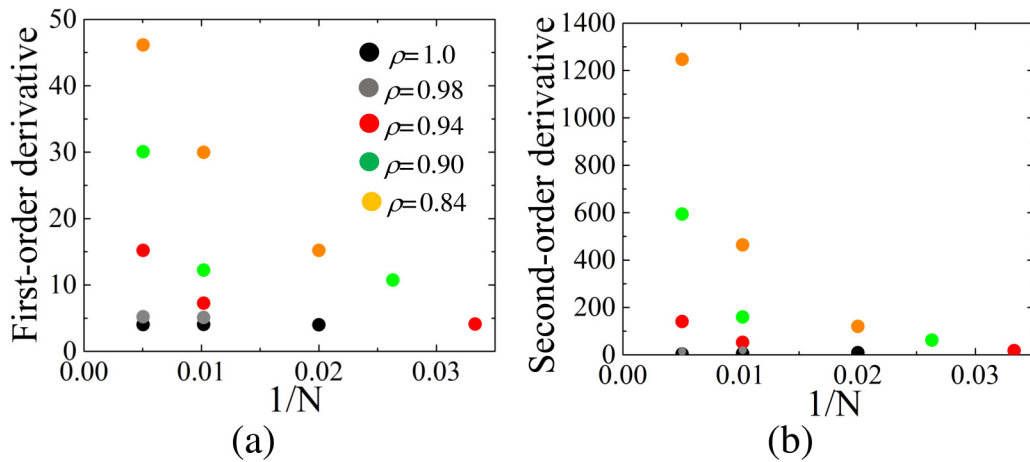


FIG. 9. Size dependence of the absolute values of the first-order (a) and second-order (b) derivatives of  $n_k$  at  $k = k_F$  for  $(U, V) = (1.0, 0.5)$ .

$|k_F - k|$  is as small as 0.016 in the nearest point and therefore,  $\alpha = 0.23$  would not be a bad estimation.

The second-order derivative shows how rapidly the curvature changes. In other words, it represents changes beyond linear behavior. The difference of  $n_k$  between two neighboring points changes rapidly when the second-order derivative is large, while  $n_k$  varies almost linearly when the second-order derivative is small. Thus, the second-order derivative is often used to represent the critical behavior, or abrupt changes beyond a linear dependence. From the current calculations, we can conclude that the second-order derivative of  $n_k$  diverges in the thermodynamic limit in the heavily doped regime. However, the change of  $n_k$  itself is finite at  $k = k_F$ , and therefore  $\frac{d^2 n_k}{dk^2} (\Delta k)^2$  should be finite there also. So, the second-order derivative can still be used to represent the critical change of  $n_k$ . In Fig. 11, we show the doping dependence of  $|\frac{d^2 n_k}{dk^2}| (\Delta k)^2$  at  $k = k_F$  for  $N = 198$ . Interestingly, this doping dependence qualitatively agrees with the experimentally observed doping dependence of the Pauli susceptibility [4]. This coincidence is

natural, because the amplitude of a singular change at  $k = k_F$  will correspond to the weight of a TLL which can give the Pauli susceptibility. Thus, the present numerical calculations can explain both the IR and Pauli susceptibility experimental results consistently.

Finally, we discuss how a metallic state with Pauli susceptibility can be realized with lattice solitons. A possible explanation is shown schematically in Fig. 12. Solitons are known to form midgap states between the valence and conduction bands [2]. With increasing doping, these mid gap states form a so-called soliton band. In the classical adiabatic approximation, this soliton band is isolated from both the valence and conduction bands, even in the heavily doped regime. In other words, a metallic state cannot be realized in the framework of the classical lattice approximation (left panel of Fig. 12). In the middle panel of Fig. 12, we show schematically the nonadiabatic effects of the lattice. For the Res-HF wave function, we superpose different coherent states which make different lattice structures. The electron motion is affected by the potential-energy landscape created by these different lattice structures. In a previous paper [10], one of

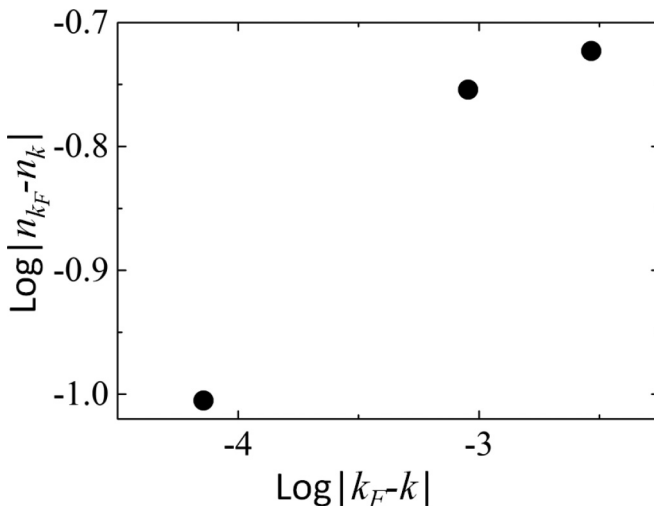


FIG. 10.  $|k_F - k|$  dependence of  $|n_{k_F} - n_k|$  for  $N = 198$ ,  $N_e = 166$ , and  $(U, V) = (1.0, 0.5)$  in log-log scale.

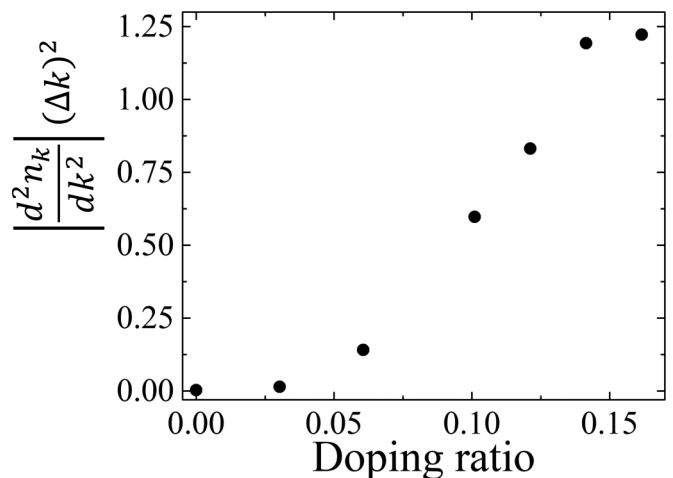


FIG. 11. Doping dependence of  $|\frac{d^2 n_k}{dk^2}| (\Delta k)^2$  at  $k = k_F$  for  $(U, V) = (1.0, 0.5)$  and  $N = 198$ .

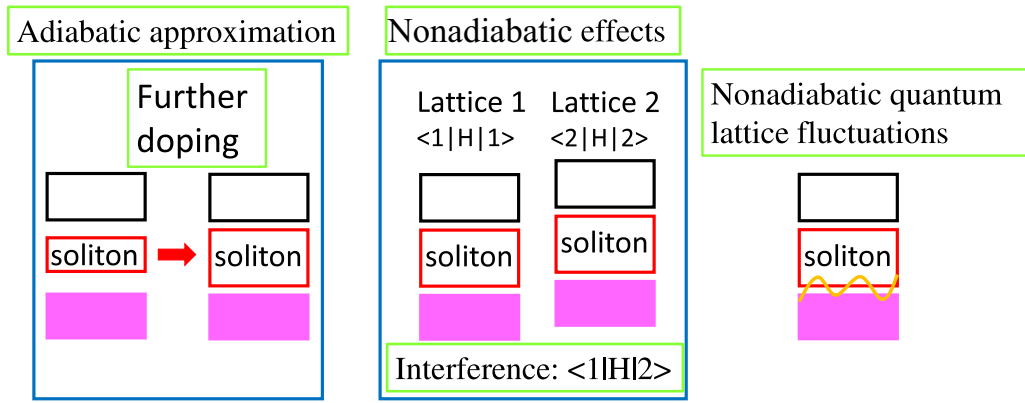


FIG. 12. Schematic representation of the mechanism for the closing of the gap by quantum fluctuations due to charged lattice solitons.

the authors (A.T.) included part of the nonadiabatic potential energy which comes from the statistical average over different lattice structures. However, the interference effects of these different lattice structures were neglected. We believe that the interference effects are important for realizing the metallic state, for the following reason. When we neglect the interference effects, electrons feel the potential energy created by only one lattice configuration. In that case, even if the bottom of the soliton band in lattice 1 is lower than the top of the valence band in lattice 2, electrons cannot move freely without a gap, because in each lattice configuration, the soliton band is isolated from both the valence and conduction bands. By taking interference effects into account, electrons can move under the potential-energy landscape created by all of the lattice configurations. As a result, the gap is really closed, and a metallic state is realized, as shown in the right panel of Fig. 12.

To support this discussion, we show in Fig. 13  $N_S$  dependence of  $n_k$  for  $N = 198$ ,  $N_e = 178$ , and  $(U, V) = (1.0, 0.5)$ .  $n_k$  does not have a singularity at  $k = k_F$  in the HF and projected HF ( $N_S = 1$ ) approximations. This means that the system cannot be metallic or a TLL if many-body effects are not included enough. In the case of the projected

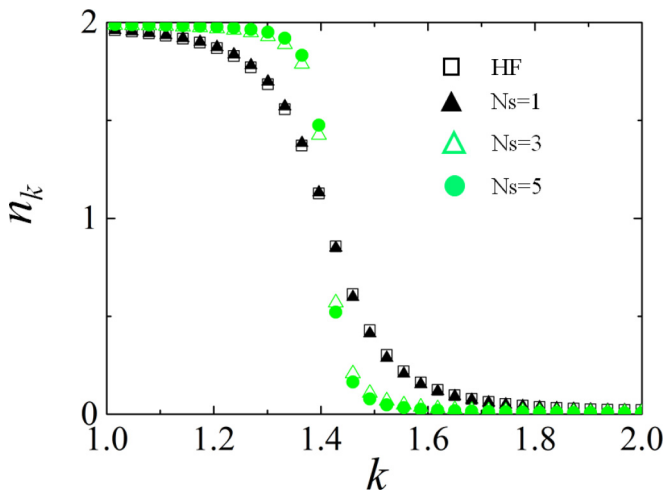


FIG. 13.  $N_S$  dependence of  $n_k$  for  $(U, V) = (1.0, 0.5)$  and  $N_e = 178$ .

HF approximation, we can include many-body effects due to the symmetry projections. However, each symmetry projected state has the same band structure because the electronic state and lattice are simultaneously translated or rotated. Therefore interference among these symmetry projected states does not reduce the gap significantly. On the other hand, a singularity at  $k = k_F$  appears when the number of Slater determinants and coherent states is increased. The present result indicates that many-body effects make the system metallic or a TLL. These many-body effects are mainly caused by lattice fluctuations beyond the adiabatic approximation, because the system becomes metallic even for  $(U, V) = (0, 0)$ . Furthermore, as mentioned above, strong electron correlations do not favor the charged lattice solitons.

The disappearance of the gap would be restricted to the heavily doped regime, where the gap between the soliton and valence (or conduction) bands is small. In the lightly doped regime, the gap is still large, and quantum fluctuations cannot close it.

Previous DMRG calculations clarified that the electron correlations make the equidistant lattice stable. In fact, as mentioned above, lattice dimerization vanishes also in our calculations when  $U/t$  becomes larger than about 1.5. The equidistant lattice makes the system metallic, but cannot explain the IR experiments. Therefore, the present results strongly suggest that the quantum lattice fluctuations, rather than electron correlations, are important to explain the IR experiments and Pauli susceptibility correctly.

In experiments, the dopant ions exist near the polyacetylene chains. Some researchers [24,25] have suggested that the random placement of such dopants might make the gap vanish. In fact, we can imagine that a finite density of states (DOS) might be induced between the soliton and valence bands, if the statistical average is taken over the DOSs with different configurations of dopants. However, in this scenario, there is no interference among different dopant configurations (imagine the average of  $\langle 1|H|1 \rangle$  and  $\langle 2|H|2 \rangle$  in Fig. 12), and there would be a finite gap in the DOS for each configuration. Therefore, the total gapless DOS caused by such statistical averaging does not always lead to a metallic state. In fact, discrepancies between the pseudogap behavior in the DOS and the large optical gap in light absorption spectra have been pointed out for strongly correlated electron systems [26–28]. In contrast, we have shown that polyacetylene can become

metallic intrinsically by doping without dopant potential. Such a metallic state could be realized also with electric-field doping where there are no dopant ions. This technique has recently been applied to many polymers, including polythiophene, with nondegenerate dimerized lattices. Polarons and bipolarons are the carriers in such conducting polymers. It is an interesting question whether quantum lattice fluctuations due to polarons or bipolarons can make the gap vanish in the absence of dopant ions. Quantum lattice fluctuations in nondegenerate polymers will be reported elsewhere in the near future.

#### IV. SUMMARY

We have introduced a tractable numerical method that can efficiently describe quantum electron and lattice fluctuations simultaneously. The wave functions are constructed by the superposition of direct products of Slater determinants for electrons and the coherent states of phonons. The lattice is thus naturally treated beyond the adiabatic approximation. By analyzing the structures of the Slater determinants and coherent states, we can visualize the quantum fluctuations. The method has been applied to a one-dimensional electron

system with SSH-type electron-phonon coupling to clarify the electronic states of doped polyacetylene. It has been shown that the charged lattice solitons are formed by doping, and that lattice dimerization and solitons persist with heavy doping up to at least 16%. Then, from the  $k$  dependence of the density of states,  $n_k$ , we have shown that the TLL contribution increases with increasing doping. The size dependence of the first- and second-order derivatives of  $n_k$  clearly indicate that  $n_k$  has a singularity at  $k = k_F$  in the heavily doped regime. This means that the system becomes a TLL. We have roughly estimated the critical exponent for  $n_k$  in the vicinity of  $k = k_F$  as  $\alpha = 0.23$  at  $\rho = 0.16$ . Quantum lattice fluctuation effects which are not included in the adiabatic approximation are responsible for the vanishing of the gap between the soliton and valence (or conduction) bands. These results are consistent with both the IR and Pauli susceptibility experiments. Thus, the present calculations have succeeded in describing the electronic states of polyacetylene.

#### ACKNOWLEDGMENT

We thank L. R. Nemzer from Edanz Group ([www.edanzediting.com/ac](http://www.edanzediting.com/ac)) for editing a draft of this manuscript.

- 
- [1] C. K. Chiang, C. R. Fincher, Jr., Y. W. Park, A. J. Heeger, H. Shirakawa, E. J. Louis, S. C. Gau, and A. G. MacDiarmid, *Phys. Rev. Lett.* **39**, 1098 (1977).
  - [2] W. P. Su, J. R. Schrieffer, and A. J. Heeger, *Phys. Rev. Lett.* **42**, 1698 (1979).
  - [3] A. J. Epstein, H. Rommelmann, R. Bigelow, H. W. Gibson, D. M. Hoffman, and D. B. Tanner, *Phys. Rev. Lett.* **50**, 1866 (1983).
  - [4] S. Ikehata, J. Kaufer, T. Woerner, A. Pron, M. A. Druy, A. Sivak, A. J. Heeger, and A. G. MacDiarmid, *Phys. Rev. Lett.* **45**, 1123 (1980).
  - [5] E. Jeckelmann and D. Baeriswyl, *Synth. Met.* **65**, 211 (1994).
  - [6] E. Jeckelmann, *Phys. Rev. B* **57**, 11838 (1998).
  - [7] D. B. Tanner, G. L. Dollb, A. M. Raob, P. C. Eklundb, G. A. Arbucklec, and A. G. MacDiarmid, *Synth. Met.* **141**, 75 (2004).
  - [8] K. Kaneto, S. Hayashi, S. Ura, and K. Yoshino, *J. Phys. Sci. Jpn.* **54**, 1146 (1985).
  - [9] K. Mizoguchi, M. Honda, N. Kachi, Fi. Shimizu, H. Sakamoto, and K. Kume, *Solid State Commun.* **96**, 333 (1995).
  - [10] A. Takahashi, *Phys. Rev. B* **46**, 11550 (1992).
  - [11] K. Shida, Y. Watanabe, H. Gomi, A. Takahashi, and N. Tomita, *J. Phys. Soc. Jpn.* **84**, 124803 (2015).
  - [12] H. Fukutome, *Prog. Theor. Phys.* **80**, 417 (1988).
  - [13] N. Kawakami and S. K. Yang, *Prog. Theor. Phys. Suppl.* **107**, 59 (1992).
  - [14] N. Tomita and S. Watanabe, *Phys. Rev. Lett.* **103**, 116401 (2009).
  - [15] N. Tomita, *Phys. Rev. B* **69**, 045110 (2004).
  - [16] W. Barford and R. J. Bursill, *Phys. Rev. B* **73**, 045106 (2006).
  - [17] M. Weber, F. F. Assaad, and M. Hohenadler, *Phys. Rev. B* **91**, 245147 (2015).
  - [18] S. Beyl, F. Goth, and F. F. Assaad, *Phys. Rev. B* **97**, 085144 (2018).
  - [19] I. Harada, Y. Furukawa, M. Tasumi, H. Shirakawa, and S. Ikeda, *J. Chem. Phys.* **73**, 4746 (1980).
  - [20] H. Fukutome, *J. Mol. Struct.: THEOCHEM* **188**, 337 (1989).
  - [21] M. Sasai and H. Fukutome, *Solid State Commun.* **51**, 609 (1984).
  - [22] M. Sasai and H. Fukutome, *Solid State Commun.* **58**, 735 (1986).
  - [23] S. Kivelson and D. E. Heim, *Phys. Rev. B* **26**, 4278 (1982).
  - [24] E. M. Conwell and S. Jeyadev, *Phys. Rev. Lett.* **61**, 361 (1988).
  - [25] K. Harigaya and A. Terai, *Solid State Commun.* **78**, 335 (1991).
  - [26] S. Shin, Y. Tezuka, T. Kinoshita, T. Ishii, T. Kashiwakura, M. Takahashi, and Y. Suda, *J. Phys. Soc. Jpn.* **64**, 1230 (1995).
  - [27] G. A. Thomas, D. H. Rapkine, S. A. Carter, A. J. Millis, T. F. Rosenbaum, P. Metcalf, and J. M. Honig, *Phys. Rev. Lett.* **73**, 1529 (1994).
  - [28] N. Tomita and K. Nasu, *Solid State Commun.* **111**, 175 (1999).